Design considerations for a high power, ultrabroadband optical parametric chirped-pulse amplifier

M. J. Prandolini, [1*] **R. Riedel,** [1,2] **M. Schulz,** [1,2,3] **A. Hage,** [3,4] **H. Höppner,** [3] **and F. Tavella** [1]

[1]*Helmholtz-Institut Jena, Fröbelstieg 3, D-07743 Jena, Germany*
[2]*Universität Hamburg, Luruper Chaussee 149, D-22761 Hamburg, Germany*
[3]*Deutsches Elektronensynchrotron DESY, Notkestrasse 85, D-22607 Hamburg, Germany*
[4]*Queens University Belfast, University Road Belfast, BT7 1NN, United Kingdom*

[*]*Mark.Prandolini@desy.de*

Abstract: A conceptual design of a high power, ultrabroadband optical parametric chirped-pulse amplifier (OPCPA) was carried out comparing nonlinear crystals (LBO and BBO) for 810 nm centered, sub-7.0 fs pulses with energies above 1 mJ. These amplifiers are only possible with a parallel development of kilowatt-level OPCPA-pump amplifiers. It is therefore important to know good strategies to use the available OPCPA-pump energy efficiently. Numerical simulations, including self- and cross-phase modulation, were used to investigate the critical parameters to achieve sufficient spectral and spatial quality. At high output powers, thermal absorption in the nonlinear crystals starts to degrade the output beam quality. Strategies to minimize thermal effects and limits to the maximum average power are discussed.

OCIS codes: (190.4410) Nonlinear optics, parametric processes; (190.4400) Nonlinear optics, materials.

References and links

1. J. Rothhardt, S. Hädrich, E. Seise, M. Krebs, F. Tavella, A. Willner, S. Düsterer, H. Schlarb, J. Feldhaus, J. Limpert, J. Rossbach, and A. Tünnermann, "High average and peak power few-cycle laser pulses delivered by fiber pumped OPCPA system," Opt. Express **18**, 12719–12726 (2010).
2. F. Tavella, A. Willner, J. Rothhardt, S. Hädrich, E. Seise, S. Düsterer, T. Tschentscher, H. Schlarb, J. Feldhaus, J. Limpert, A. Tünnermann, and J. Rossbach, "Fiber-amplifier pumped high average power few-cycle pulse noncollinear OPCPA," Opt. Express **18**, 4689–4694 (2010).
3. J. Rothhardt, S. Demmler, S. Hädrich, J. Limpert, and A. Tünnermann, "Octave-spanning OPCPA system delivering CEP-stable few-cycle pulses and 22 W of average power at 1 MHz repetition rate," Opt. Express **20**, 10870–10878 (2012).
4. R. Riedel, M. Schulz, M. J. Prandolini, A. Hage, H. Höppner, T. Gottschall, J. Limpert, M. Drescher, and F. Tavella, "Long-term stabilization of high power optical parametric chirped-pulse amplifiers," Opt. Express **21**, 28987–28999 (2013).
5. B. Faatz, N. Baboi, V. Ayvazyan, V. Balandin, W. Decking, S. Duesterer, H.-J. Eckoldt, J. Feldhaus, N. Golubeva, K. Honkavaara, M. Koerfer, T. Laarmann, A. Leuschner, L. Lilje, T. Limberg, D. Noelle, F. Obier, A. Petrov, E. Ploenjes, K. Rehlich, H. Schlarb, B. Schmidt, M. Schmitz, S. Schreiber, H. Schulte-Schrepping, J. Spengler, M. Staack, F. Tavella, K. Tiedtke, M. Tischer, R. Treusch, M. Vogt, A. Willner, J. Bahrdt, R. Follath, M. Gensch, K. Holldack, A. Meseck, R. Mitzner, M. Drescher, V. Miltchev, J.Rönsch-Schulenburg, J. Rossbach, "Flash II: Perspectives and challenges," Nucl. Instr. Meth. A **635**, S2–S5 (2011).
6. H. Redlin, A. Al-Shemmary, A. Azima, N. Stojanovic, F. Tavella, I. Will, and S. Düsterer, "The FLASH pump-probe laser system: Setup, characterization and optical beamlines," Nucl. Instr. Meth. A **635**, S88–S93 (2011).

#198661 - $15.00 USD Received 30 Sep 2013; revised 27 Nov 2013; accepted 27 Nov 2013; published 16 Jan 2014

7. G. Sansone, F. Calegari, and M. Nisoli, "Attosecond technology and science," IEEE J. Sel. Topics Quant. Elect. **18**, 507–519 (2012).
8. S. Banerjee, M. Baudisch, J. Biegert, A. Borot, A. Borzsonyi, D. Charalambidis, T. Ditmire, Zs. Diveki, P. Dombi, K. Ertel, M. Galimberti, J. A. Fülöp, E. Gaul, C. Haeffner, M. Hemmer, C. Hernandez-Gomez, M. Kalashnikov, D. Kandula, A. P. Kovacs, R. Lopez-Martens, P. Mason, I. Márton, I. Musgrave, K. Osvay, M. Prandolini, E. Racz, P. Racz, R. Riedel, I. N. Ross, J.-P. Rosseau, M. Schulz, F. Tavella, A. Thai, I. Will, "Conceptual design of the laser system for the attosecond light pulse source," in "CLEO:2013 Technical Digest © OSA," (2013).
9. M. Schulz, R. Riedel, A. Willner, T. Mans, C. Schnitzler, P. Russbueldt, J. Dolkemeyer, E. Seise, T. Gottschall, S. Hädrich, S. Duesterer, H. Schlarb, J. Feldhaus, J. Limpert, B. Faatz, A. Tünnermann, J. Rossbach, M. Drescher, and F. Tavella, "Yb:YAG Innoslab amplifier: efficient high repetition rate subpicosecond pumping system for optical parametric chirped pulse amplication," Opt. Lett. **36**, 2456–2458 (2011).
10. M. Schulz, R. Riedel, A. Willner, S. Düsterer, M. J. Prandolini, J. Feldhaus, B. Faatz, J. Rossbach, M. Drescher, and F. Tavella, "Pulsed operation of a high average power Yb:YAG thin-disk multipass amplifier," Opt. Express **20**, 5038–5043 (2012).
11. B. C. Stuart, M. D. Feit, A. M. Rubenchik, B. W. Shore, and M. D. Perry, "Laser-induced damage in dielectrics with nanosecond to subpicosceond pulses," Phys. Rev. Lett. **74**, 2248–2251 (1995).
12. S. T. Lin, Y. Y. Lin, Y. C. Huang, A. C. Chiang, and J. T. Shy, "Observation of thermal-induced optical guiding and bistability in a mid-IR continuous-wave, singly resonant optical parametric oscillator," Opt. Lett. **33**, 2338–2340 (2008).
13. M. Vainio, J. Peltola, S. Persijn, F. J. M. Harren, and L. Halonen, "Thermal effects in singly resonant continuous-wave optical parametric oscillators," Appl. Phys. B **94**, 411–427 (2009).
14. J. Rothhardt, S. Demmler, S. Hädrich, T. Peschel, J. Limpert, and A. Tünnermann, "Thermal effects in high average power optical parametric amplifiers," Opt. Lett. **38**, 763–765 (2013).
15. R. Akbari and A. Major, "Optical, spectral and phase-matching properties of BIBO, BBO and LBO crystals for optical parametric oscillation in the visible and near-infrared wavelength ranges," Laser Phys. **23**, 035401 (2013).
16. D. N. Nikogosyan, *Nonlinear Optical Crystals: A Complete Survey* (Springer, 2005).
17. A. V. Smith, *SNLO nonlinear optics code (Ver. 60)*, AS-Photonics, Albuquerque, USA (2013).
18. I. N. Ross, P. Matousek, G. H. C. New, and K. Osvay, "Analysis and optimization of optical parametric chirped pulsed amplification," J. Opt. Soc. Am. B **19**, 2945–2956 (2002).
19. D. N. Schimpf, J. Rothhardt, J. Limpert, A. Tünnermann, and D. C. Hanna, "Theoretical analysis of the gain bandwidth for noncollinear parametric amplification of ultrafast pulses," J. Opt. Soc. Am. B **24**, 2837–2846 (2007).
20. J. Moses and S.-W. Huang, "Conformal profile theory for performance scaling of ultrabroadband optical parametric chirped pulse amplification," J. Opt. Soc. Am. B **28**, 812–831 (2011).
21. S. Witte, R. T. Zinkstok, W. Hogervorst, and K. S. E. Eikema, "Numerical simulations for performace optimization of a few-cycle terawatt NOPCPA system," Appl. Phys. B **87**, 677–684 (2007).
22. R. W. Boyd, *Nonlinear Optics* (Academic Press, 2008).
23. D. Zhang, Y. Kong, and J.-Y. Zhang, "Optical parametric properties of 523-nm-pumped beta-barium-borate near the infrared absorption edge," Opt. Comm. **184**, 485–491 (2000).
24. M. Bache, H. Guo, B. Zhou, and X. Zeng, "The anisotropic Kerr nonlinear refractive index of the beta-barium borate (β-BaB_2O_4) nonlinear crystal," Optical Materials Express **3**, 357–382 (2013).
25. K. Kato, "Temperature-Tuned 90° Phase-Matching Properties of LiB_3O_5," IEEE J. Quant. Elect. **30**, 2950–2952 (1994).
26. M. Sheik-Bahae and M. Ebrahimzadeh, "Measurements of nonlinear refraction in the second-order $\chi^{(2)}$ materials $KTiOPO_4$, $KNbO_3$, β-BaB_2O_4, and LiB_3O_5," Opt. Comm. **142**, 294–298 (1997).
27. A. Thai, C. Skrobol, P. K. Bates, G. Arisholm, Z. Major, F. Krausz, S. Karsch, and J. Biegert, "Simulations of petawatt-class few-cycle optical parametric chirped-pulse amplification including nonlinear refractive index effects," Opt. Lett. **35**, 3471–3473 (2010).
28. C. Chen, Y. Wu, A. Jiang, B. Wu, G. You, R. Li, and S. Lin, "New nonlinear-optical crystal: LiB_3O_5," J. Opt. Soc. Am. B **6**, 616–621 (1989).
29. J. Bromage, J. Rothhardt, S. Hädrich, C. Dorrer, C. Jocher, S. Demmler, J. Limpert, A. Tünnermann, and J. D. Zuegel, "Analysis and suppression of parasitic processes in noncollinear optical parametric amplifiers," Opt. Express **19**, 16797–16808 (2011).
30. A. E. Siegman, "How to (maybe) measure laser beam quality," OSA TOPS **17**, 184–199 (1998).
31. A. L. Oien, I. T. McKinnie, P. Jain, N. A. Russell, D. M. Warrington, and L. A. W. Gloster, "Efficient, low-threshold collinear and noncollinear β-barium borate optical parametric oscillators," Opt. Lett. **22**, 859–861 (1997).
32. S. Demmler, J. Rothhardt, S. Hädrich, J. Bromage, J. Limpert, and A. Tünnermann, "Control of nonlinear spectral phase induced by ultrabroadband optical parametric amplification," Opt. Lett. **19**, 3933–3935 (2012).
33. S. Seidel and G. Mann, "Numerical modeling of thermal effects in nonlinear crystals for high average power second harmonic generation," Proc. SPIE 2989 (1997).

#198661 - $15.00 USD Received 30 Sep 2013; revised 27 Nov 2013; accepted 27 Nov 2013; published 16 Jan 2014

1. Introduction

Optical parametric chirped-pulse amplification (OPCPA) is presently the most promising method for the amplification of ultrabroadband optical pulses to high average powers. This technique has already been demonstrated in the amplification to tens of watts with a repetition rate in the range between tens of kHz to MHz [1–4]. Currently, OPCPA systems are finding application at high repetition rate free-electron lasers (FELs); for example, the seeding of the new FEL FLASH 2 in Hamburg, Germany [5] and for pump-probe lasers [6]. In these applications, the OPCPA systems will operate in burst-mode (FLASH currently operates with a burst structure of up to 1 MHz for 800 μs at 10 Hz). In the field of attosecond technology and science [7], OPCPAs can be used as driving amplifiers for secondary sources. For example, the Extreme Light Infrastructure – Attosecond Light Pulse Source (ELI-ALPS) in Szeged, Hungary is planing a high power OPCPA operating at 100 kHz with a pulse energy of 5 mJ and a duration of sub-5 fs (1 mJ and sub-7 fs is planed in a first phase) [8]. All these applications require significant development to the OPCPA setup [4] and to the OPCPA-pump laser [9, 10].

Currently, one of the major restrictions to the development of high power OPCPA systems is the availability of reliable OPCPA-pump amplifiers. Pump pulse durations should be in the sub/few picosecond range providing tens to hundreds of millijoules of energy. Short pump pulses not only reduce the required stretching and compression of the ultrabroadband signal pulse, but also allow for a higher pump intensity in the nonlinear crystals before the damage threshold is reached [11]. These laser parameters can potentially be achieved using Yb-based solid-state laser technology. A typical system usually consists of a Yb-doped fiber amplifier as a front-end combined with a Yb:YAG Innoslab amplifier system [9] and/or a Yb:YAG thin-disk amplifier for low gain, high average power amplification [10]. Presently, OPCPA-pump amplifiers operating in the kilowatt level do not exist, but are planned for the near future. In the design of an ultrabroadband, high power OPCPA system, the OPCPA-pump will be the most costly and energy consuming part of the system. Therefore, the design of an OPCPA should try to optimize the use of the available pump energy. This also keeps initial and running costs to a minimum, and additionally, by reducing the total pump power requirements, the total thermal load and heat dissipation are also minimized.

Another restriction to increasing the average power of ultrabroadband OPCPAs is thermal effects, caused by the absorption of the pump, signal and idler pulses within the nonlinear crystals. Thermal effects, such as thermal lensing and bistability, have already been observed in continuous-wave optical parametric oscillators (OPOs) [12, 13]. Recently, thermal effects have been experimentally observed in OPCPAs using the nonlinear crystal β-barium borate (BBO) [14]. However, because of the lack of powerful pump lasers, or due to their operation in burst-mode, thermal effects have not been studied in detail in OPCPA systems.

Amongst the wide variety of nonlinear crystals, BBO and lithium triborate (LBO) are well-established materials [15], which are used in the OPCPA of ultrabroadband, high repetition laser pulses. Other crystals worth mentioning are the introduction of bismuth triborate (BIBO) and yttrium calcium oxyborate (YCOB) [16]. A summary of some important parameters is given in Table 1. Compared to BBO and LBO, BIBO has a larger nonlinear coefficient, while YCOB has a smaller nonlinear coefficient. At very high pump powers, where the thermal load on the crystal becomes important, LBO might be the best choice, because of its low absorption at the pump wavelength (515 nm). However, if the crystal has a thermal gradient, its low temperature tolerance would destroy phase matching. In contrast, BBO and YCOB crystals with higher temperature tolerances would be more tolerant to temperature changes across the crystal. A comparison of the gain bandwidth for crystals LBO, BBO, BIBO and YCOB [15, 16], shows that the broadest bandwidth for amplification is still offered by BBO and LBO: these two crystals are investigated in detail in this work.

#198661 - $15.00 USD Received 30 Sep 2013; revised 27 Nov 2013; accepted 27 Nov 2013; published 16 Jan 2014

Table 1. Properties of nonlinear crystals: d_{eff} effective nonlinear optical coefficient, ρ walk-off angle, TT temperature tolerance, AT angular tolerance, $\alpha_{515\text{ nm}}$ absorption coefficients at 515 nm, and $\overline{\kappa}$ thermal conductivity (averaged over the crystal axes). Values given for $\lambda_{\text{pump}} = 515$ nm and $\lambda_{\text{signal}} = 800$ nm. These values are taken from [16, 17]. (Note: Critical for this work are the values of α_{515}, which can greatly vary in the literature [16]. The values given in the table are considered worst-case upper limits.)

	d_{eff} [pm/V]	ρ [mrad]	TT [K cm]	AT [mrad cm]	$\alpha_{515\text{ nm}}$ [cm^{-1} %]	$\overline{\kappa}$ [Wm^{-1}K^{-1}]
BBO	2.0	55.8	39.7	0.56	< 1	1.33
LBO	1.0	7.06	6.8	4.54	< 0.1	3.5
BIBO	3.0	25.0	2.74	1.15	–	–
YCOB	0.36	32.1	110.9	0.94	–	2.6

An outline of this paper is organized as follows. First, a brief overview of the numerical simulation is given including the literature sources for the nonlinear material parameters for both LBO and BBO crystals. Second, a scheme for a three-stage OPCPA system is presented describing the starting and final pulse parameters. The aim of the simulations was to achieve pulse energies above 1 mJ with a bandwidth supporting sub-7 fs pulses, and to provide sufficient spatial beam quality determined by its M^2-value. From these results the pump-to-signal efficiencies and compressible pulse durations for both LBO and BBO are derived. Third, because many applications require both good near and far field beam characteristics, the critical parameters required for high spatial beam quality are analyzed. Fourth, spectral phase effects (up to the fourth order) of the nonlinear processes are discussed for both the optical parametric amplification and phase modulation. Finally, the energetics of the complete amplifier and possible maximum average power, which is ultimately restricted by thermal effects, will be discussed. The maximum power, through a single stage nonlinear crystal, is difficult to estimate, because there needs to be an exact thermal model of the crystal holder. In addition, the temperature dependence of the many optical material parameters is not well known, especially in the case of a strong varying temperature profile across the crystals. We therefore restrict our discussion to how to achieve maximum average power for a single stage and give an estimate for the maximum average power at which thermal effects start to change the optical properties of the amplifier.

2. Numerical modeling and material parameters

Existing analytical solutions of the non-collinear optical parametric amplifier (NOPA) processes provide an accurate estimate of the gain bandwidth, but generally neglect dispersion and walk-off effects [18–20]. Numerical methods provide good estimates for the pulse energetics and closely reflect experimentally chosen parameters, such as, pulse energy, pulse duration, spectrum and phase [18, 21]. Here, a 2D-model was developed with the z-axis along the signal propagation axis and one transverse direction (x-axis) formed in the plane between the signal and pump axes. The nonlinear coupled equations, Eq. (1), within the slowly varying envelope approximation ($E = \frac{1}{2}(A\exp(i(\omega_0 t - k_0 z)) + \text{c.c.})$), describing the signal (S), pump (P) and idler (I) pulses at center frequency ω_0 and wavenumber k_0 were solved using a fourth-order Runge-Kutta split-step Fourier algorithm. The nonlinear part of these equations are given below:

$$\begin{aligned}
\frac{\mathrm{d}A_S}{\mathrm{d}z} &= -i\frac{\omega_S d_{\text{eff}}}{n_S c}A_I^* A_P e^{i\Delta kz} - i\frac{n_{2S}k_S}{n_S}(|A_S|^2 + \gamma_{SI}|A_I|^2 + \gamma_{SP}|A_P|^2)A_S \\
\frac{\mathrm{d}A_I}{\mathrm{d}z} &= -i\frac{\omega_I d_{\text{eff}}}{n_I c}A_S^* A_P e^{i\Delta kz} - i\frac{n_{2I}k_I}{n_I}(|A_I|^2 + \gamma_{SI}|A_S|^2 + \gamma_{SP}|A_P|^2)A_I
\end{aligned}$$

#198661 - $15.00 USD Received 30 Sep 2013; revised 27 Nov 2013; accepted 27 Nov 2013; published 16 Jan 2014

$$\frac{dA_P}{dz} = -\frac{\alpha_{515}}{2}A_P - i\frac{\omega_P d_{\text{eff}}}{n_P c}A_S A_I e^{-i\Delta kz} - i\frac{n_{2P}k_P}{n_P}(|A_P|^2 + \gamma_{PS}|A_S|^2 + \gamma_{PI}|A_I|^2)A_P \quad (1)$$

where $\Delta k = k_S + k_I - k_P$ is the wavenumber mismatch, d_{eff} the nonlinear optical coefficient, n_m ($m = S, I, P$) refractive indices, α_{515} is the absorption coefficient (Table 1), n_{2m} the nonlinear refractive indices and γ_{PS} and γ_{IS} are the correction coefficients accounting for the cross-phase modulation effects [22]. The last terms on the right hand side represent the self- and cross-phase modulation effects, SPM and XPM, respectively. For BBO, the coefficients for the Sellmeier equations were taken from [23], and the second and third order nonlinear coefficients from [24]. For LBO, the coefficients for the Sellmeier equations were taken from [25], the second order coefficients from [15], and third order coefficients from [26]. At large pulse energies, signal and pump beams are effectively collimated (i.e. a very long confocal length compared to the crystal length). Under these conditions, refractive terms can be neglected. The linear terms (not shown), consisting of dispersion up to the fourth order, attenuation (see Section 6), and all translations along the *x*-axis for the signal, idler and pump pulses, were carried out in the Fourier domain.

For the interpretation of the results, the nonlinear phase accumulations are usually summarized with a single parameter: the *B*-integral. In this work, we modified the standard textbook definition to include SPM and XPM. Thus, the *B*-integral can be written as:

$$B_P = \frac{2\pi}{\lambda_P}\int_0^l n_{2P}(I_P(z) + \gamma_{PS}I_S(z) + \gamma_{PI}I_I(z))dz, \quad (2)$$

where l is the length of the crystal and the intensity can be derived from $I_m = \frac{1}{2}n_m\varepsilon_0 c_0|A_m|^2$, where n_m ($m = S, I, P$). The *B*-integral for the signal and idlers pulses could be correspondingly derived. However, this parameter is only useful in the interpretation of narrow band pulses, for example, the pump pulse. For ultrabroadband pulses it is better to analyze the actually phase across the pulse (see Section 5). For high energy NOPA stages, there are three damaging effects of SPM and XPM: (i) spatially distorted beam profiles resulting in larger M^2-values, (ii) frequency modulation, which may cause problems in re-compressing the signal, and (iii) the phase matching condition becomes time and position dependent (i.e. $\Delta k(t,x,z)$). This final effect can reduce the bandwidth and energy of the signal pulse [27]. All three effects are included in the simulation.

Two thermal effects were also included in the simulation. For a given temperature distribution $T(x)$ across the transverse direction of the nonlinear crystal, $\Delta k(x)$ and the group velocities ($\upsilon_m(x)$, where $m = S, I, P$) become position dependent. Higher order temperature dependencies on the dispersion were not considered. Within the non-collinear optical parametric process, matching the group velocities along the direction of the signal ($\upsilon_S(x) \simeq \upsilon_I(x)\cos\Omega$, where Ω is the spatial angle between the signal and idler pulses) is important to achieve broadband amplification. Depending on the nonlinear material, a temperature distribution across the crystals can greatly reduce the amplified bandwidth and spatial beam quality.

Damage thresholds have not been measured at the pump wavelength and pulse durations used in this work. However, BBO has been demonstrated in an OPCPA at pump intensities of 300 GW/cm^2 [3], with similar pump parameters used in this simulation. In the case of LBO, its crystal structure is built of endless helices of B_3O_7, the interstices between the helices are small and can only accommodate small ions, such as Li^+. This ensures that LBO can be grown relatively free of inclusions [28]. This is not the case for BBO. In addition, LBO has a larger band gap of 7.75 eV compared to 6.2 eV for BBO, and the crystal structure of LBO is more compact, thus the production and transport of ions and electrons is more difficult even at high laser intensities. Furthermore, LBO has a Mohs hardness of 6 compared to 4 of BBO. These factors should favor LBO to be robuster with a higher damage threshold compared to BBO [28].

#198661 - $15.00 USD Received 30 Sep 2013; revised 27 Nov 2013; accepted 27 Nov 2013; published 16 Jan 2014

3. Simulation results: dispersion management, conversion efficiencies and spectra

Numerical simulations were carried out on a three-stage non-collinear optical parametric amplifier for both BBO and LBO crystals. The aim was to produce output pulse energies above 1 mJ, with a bandwidth supporting sub-7.0 fs pulses. The OPCPA-pump pulses are assumed to have an ideal Gaussian shape with parameters of 8 mJ and 600 fs FWHM. The starting pump energy was split into 0.3 mJ (P(1)) for the first stage and 7.7 mJ (P(2)) for the second and third stages, where the pump pulse was reused for the third stage (Fig. 1). From experimental experience, 0.3 mJ is chosen for the first stage, to bring the signal pulses from the nJ to µJ level. This reduces the amplified parametric fluorescence in the second and third stages, where 96% of the pump energy is used [4]. The input signal energy was 0.5 nJ with a Gaussian spatial beam profile. All stages use type I phase matching conditions: signal and idler pulse have o-polarization and the pump pulse has e-polarization. In order to avoid the problems of second order parasitic processes, tangential phase matching was used [29]. The non-collinear angles, α (between the signal and pump pulses), and θ (between the optical axis and the pump pulse), were chosen to achieve a compromise between the resulting signal gain and bandwidth, while restricting the accumulation of spatial phase of the signal pulse, which results poor beam quality. Pulse widths and spatial expansions, between stages 1 and 2, and between 2 and 3, were again chosen as a compromise between achieving the required bandwidth, and the necessary beam quality at the final output (Fig. 1). The chosen crystal thicknesses were for the three stages, $l_1 = 3.1$, $l_2 = 1.5$ and $l_3 = 1.2$ mm, and $l_1 = 1.7$, $l_2 = 0.9$, $l_3 = 0.5$ mm for LBO and BBO, respectively.

It is important to carefully consider the dispersion management throughout the system. For the applications considered here (see Introduction), the final amplified pulses would need to pass into vacuum through a window with known (positive) dispersion, spatially shaped, transported and temporally compressed before being focused. These factors of transport and final application are not addressed in this work; however, they are best served, if the pulses receive a negative chirp at the beginning. We chose to construct an input signal pulse, whose amplitude was generated from an experimental spectrum taken from a commercial ultrabroadband Ti:sapphire oscillator (Venteon, Pulse: ONE-OPCPA). In order to reduce thermal effects, the lower wavelengths were filtered out, using different cut-off values for LBO and BBO (for a detailed discussion see Section 6). The phase of the signal pulse was derived from a simulated prism-stretcher up to the fourth order (negatively chirped). For both LBO or BBO, the first stage has the longest crystal length, and therefore, due to the dispersion in the first stage, the output pulse duration might not be optimal for the second and third stages. Thus, to achieve optimal gain in the second and the third stages, the signal pulse is again negatively chirped between stages 1 and 2; this could be implemented with chirped mirrors (Fig. 1). Further flexibility and efficiency could be achieved by implementing a similar temporal stretch between the second and third stages; however, given the beam energy and the pulse width after the second stage,

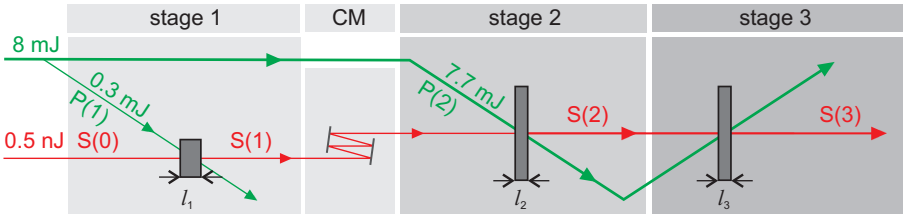

Fig. 1. Schematic of the three-stage OPCPA: pump pulses P(1) and P(2) (solid, green) and signal pulses S(0), S(1), S(2) and S(3) (solid, red); l_1, l_2 and l_3 are widths of the nonlinear crystals; CM chirped mirror.

#198661 - $15.00 USD Received 30 Sep 2013; revised 27 Nov 2013; accepted 27 Nov 2013; published 16 Jan 2014

this might be difficult to realize experimentally, and was not implemented in this design. The various chosen parameters and those generated by the simulations for LBO and BBO are given in Table 2.

Table 2. OPCPA laser pulse parameters for the pump and signal at various positions (see Fig. 1). Pulse durations τ and widths D are characterized using FWHM. Between stages 1 and 2, and between 2 and 3, the signal was spatially expanded 1:8 / 1:2 for LBO and 1:10 / 1:2 for BBO, respectively; additionally group dispersion delay of -100 fs^2 for LBO and -300 fs^2 for BBO was added temporally to the signal between stages 1 and 2.

LBO	S(0)	P(1)	S(1)	P(2)	S(2)	S(3)
I_{max} [GW/cm^2]	0.46 m	115	76.9	104	75.1	41.8
E [J]	0.5 n	0.3 m	19.4 µ	7.7 m	0.90 m	1.81 m
τ [fs]	222	600	224	600	259	227
D [mm]	0.62	0.58	0.46	3.00	2.74	4.85
M^2	1.00	1.00	1.56	1.00	1.13	1.18
BBO						
I_{max} [GW/cm^2]	0.89 m	115	77.5	104	56.2	50.1
E [J]	0.5 n	0.3 m	16.4 µ	7.7 m	0.94 m	1.92 m
τ [fs]	130	600	218	600	429	399
D [mm]	0.59	0.58	0.38	3.00	1.80	3.45
M^2	1.00	1.00	1.40	1.00	1.14	1.21

The gain curves and pump-to-signal conversion efficiencies for both LBO and BBO are given in Fig. 2(a) and 2(b), respectively. For both crystals (LBO/BBO), the gain in each stage is 39000/32800, 46/57, 2/2 for the first, second and third stages, respectively. The pump-to-signal conversion efficiency is dominated by the final two stages. Considering the large financial costs of the OPCPA-pump system, a third stage is desirable, even though some sacrifice is made in the spatial beam quality (Table 2). Spectra at S(0), S(1) and S(3) (see Fig. 1) are shown in Fig. 3(a) for LBO and Fig. 3(b) for BBO, supporting a Fourier-limited pulse of 7.00 fs and 5.82 fs, respectively. Greater bandwidths could be obtained in two ways. First, signal pulse duration can be reduced compared to be pump pulse duration. This would also unfortunately reduce the conversion efficiency. Note: if the temporal pump profile was a “flat-top”, it would be always possible to stretch the signal pulse duration to the pump pulse duration, amplifying the signal with the same pump intensity. This is not the case with a temporal Gaussian beam profile. Second, the pump intensity can be increased, and thereby reducing the length of crystal needed for gain saturation. As a result, the factor Δkz in Eq. (1) is smaller over a larger range of wavelengths [3, 18].

4. Spatial beam quality

It will be shown that the spatial quality of the signal beam is mainly dependent on the quality of the pump beam intensity and not on its spatial phase. To estimate the beam quality, M^2-values will be used, and were calculated from the near-field far-field product [30]. Since the quality of the pump beam depends on the final implementation of a pump system, the simulations were carried out with Gaussian beams. With this choice, it is possible to isolate and identify the important factors determining spatial beam quality resulting from the OPCPA stages. In addition, the results for spatial beam profiles of LBO and BBO are similar, and therefore the following discussion, showing only LBO results, can be applied to both crystals.

In Fig. 4, the near-field and far-field beam profiles along the x-axis for LBO at the end of each of the first two OPCPA stages are shown. The highest M^2-value is calculated after the

#198661 - $15.00 USD Received 30 Sep 2013; revised 27 Nov 2013; accepted 27 Nov 2013; published 16 Jan 2014

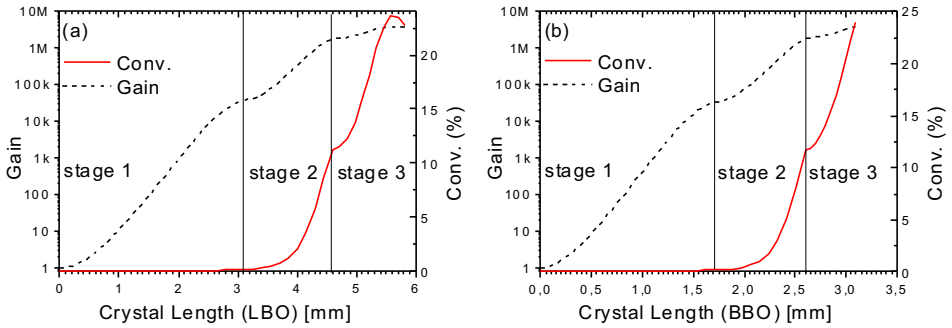

Fig. 2. Gain and conversion efficiency for the signal pulse as it passes through all three stages: LBO (a), BBO (b).

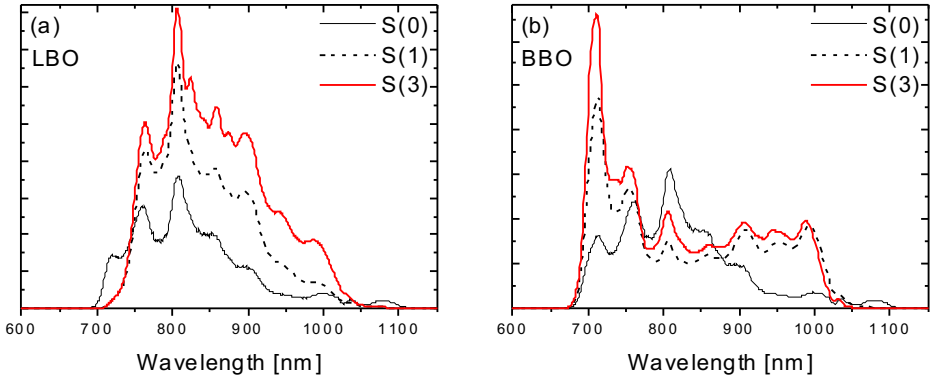

Fig. 3. Spectrum of original signal S(0), and the output spectrum of stages S(1) and S(3): LBO (a), BBO (b).

first stage (Table 2). This results from the optical parametric amplification process including spatial directional walk-off of the signal and pump pulses. This problem is most serious in the first stage, since the pulse diameters are relatively small compared to the length of the crystal. An additional factor is the choice of the phase matching geometry: tangential phase matching (TPM) or Poynting-vector walk-off compensation (PVWC) [31]. In these simulations, all three stages used TPM. Note: PVWC offers a much better beam profile; however, the signal is accompanied by SHG parasitic processes and has a slightly reduced energy. Using TPM, parasitic processes are eliminated in our region of interest (680–1100 nm) for both LBO and BBO, however, at the cost of reduced beam quality (for details see [29]).

In the second stage, the beam diameters are large compared to the crystal length, and therefore, spatial walk-off is kept to a minimum. In this case, the signal beam profile takes the form of the fresh Gaussian pump beam, provided the gain of the second stage is sufficiently large. This results in an improved beam quality, compared to the first stage (see Fig. 4 and M^2-values from Table 2). Furthermore, the spatial phase of the pump beam does not affect the beam quality of the amplified signal. This was investigated by adding an oscillatory spatial phase on the x-axis of the pump beam of the form $\exp(i\cos ax)$, where a was greater than the inverse of the

#198661 - $15.00 USD Received 30 Sep 2013; revised 27 Nov 2013; accepted 27 Nov 2013; published 16 Jan 2014

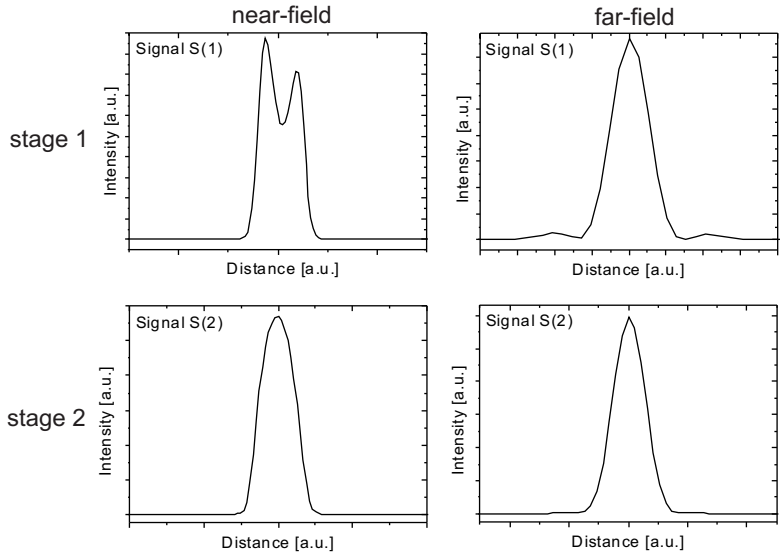

Fig. 4. Signal output intensity spatial profiles at the near-field (left column) and far-field (right column) from the first two LBO stages.

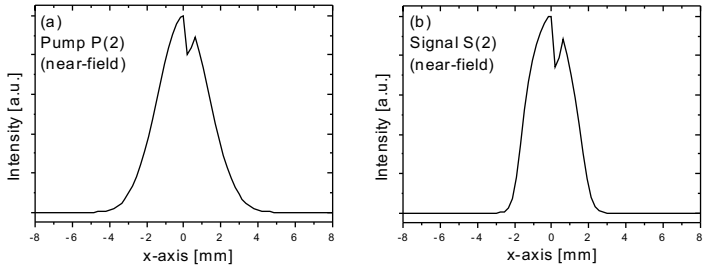

Fig. 5. Influence of spatial distortions in the output of the signal beam on a distorted input pump beam, demonstrated on the second LBO stage. (a) Input pump near-field intensity profile P(2). (b) Output signal near-field intensity profile S(2). All other parameters for the simulation of the second stage were the same as for the results in Fig. 4.

beam width. In this case, exactly the same results were achieved for the signal, but the idler was strongly modulated by the phase of the pump. In contrast, spatial distortions in the pump intensity are transferred into the signal intensity, as shown in Fig. 5. While the signal intensity profile is dominated by the pump intensity profile of the second stage, the spatial phase of the signal is predominantly accumulated on passing through the first, second, and third stages, and should be kept to a minimum.

In the final stage, the pump beam quality is very poor, because it suffered considerable depletion passing through the second stage. It could be expected from results shown in Fig. 5 that this will produce a very poor signal beam quality. The beam diameters of the third stage are similar to the second stage; however, in contrast, the gain in the final stage is small (~ 2). In addition, because the idler must again build up from zero, the degree of back conversion from signal to pump is reduced. Therefore, the spatial quality (intensity and spatial phase) of the

#198661 - $15.00 USD Received 30 Sep 2013; revised 27 Nov 2013; accepted 27 Nov 2013; published 16 Jan 2014

signal beam remains similar to its input, resulting in only a small increase in M^2 (see Table 2).

An additional factor to consider is the self-focusing of the pump beam through the crystal. The *B*-integral for the pump pulse was therefore estimated for the first, second and third stages to be 0.90, 0.38, 0.31 and 1.40, 0.63, 0.25 for LBO and BBO, respectively. For the corresponding given beam widths, self-focusing should be negligible for these values.

5. Spectral characteristics of the signal pulse

Simulations allow the possibility of isolating the cumulative effects on spectral phase resulting from dispersion (Disp.), optical parametric amplification (OPA), and from self- and cross-phase modulation (PM). Table 3 shows the starting values and the individual changes to the phase up to the fourth order, where GDD is the group delay dispersion, TOD the third-order dispersion, and FOD the fourth-order dispersion. The discussion below is qualitative, and since the results of LBO and BBO are qualitatively similar, only results from LBO are shown.

Table 3. Starting values and cumulative changes of the signal spectral phase to the group delay dispersion (GDD) (second-order dispersion), third-order dispersion (TOD) and fourth-order dispersion (FOD). ΔDisp. is the change in phase only due to dispersion within the crystal; ΔOPA is the change when optical parametric amplification is added; and, ΔPM is the change when self- and cross-phase modulation is added to the simulation. Additionally, -100 fs^2 GDD was added between stages 1 and 2 using a chirped mirror (CM).

	GDD [fs^2]	TOD [fs^3]	FOD [fs^4]
Stage 1			
Starting Values	-494.5	-665.0	-1900.6
ΔDisp.	133.2	132.4	-77.6
ΔOPA	-32.0	180.8	1150.1
ΔPM	-0.1	-17.9	-78.1
Stage 2	-100 (CM)		
Starting Values	-493.4	-369.7	-906.2
ΔDisp.	64.4	64.1	-37.6
ΔOPA	-12.1	49.6	277.9
ΔPM	0.0	-1.5	-35.4
Stage 3			
Starting Values	-441.1	-257.5	-701.3
ΔDisp.	52.9	52.5	-30.8
ΔOPA	-1.2	42.5	30.4
ΔPM	-1.0	-0.9	12.6
Final	-390.4	-163.4	-689.1

The active OPA process adds spectral phase to the signal (Table 3), and can be qualitatively understood using an analytical model, not including dispersion and walk-off effects, given by ([18], Eq. 10)

$$\Delta\phi = \frac{\Delta k}{2}\int \frac{f\,dz}{f+\gamma_S^2} \tag{3}$$

where $f = 1 - I_P(z)/I_P(0)$, $\gamma_S = \omega_P I_S(0)/(\omega_S I_P(0))$; and $I_S(z)$ and $I_P(z)$ are the intensities of the signal and pump, respectively. From Eq. (3), changes in the spectral phase can be minimized for a given Δk by using shorter crystals, increasing the ratio $I_S(0)/I_P(0)$ and by keeping pump depletion close to zero. The latter is not possible, if pump-to-signal conversion efficiency is maximized. Thus the greatest spectral phase changes are experienced in the first stage, which

#198661 - $15.00 USD Received 30 Sep 2013; revised 27 Nov 2013; accepted 27 Nov 2013; published 16 Jan 2014

has the longest crystal and the smallest $I_S(0)/I_P(0)$ ratio (see Table 3). The ratios between GDD, TOD and FOD can be modified by changing the wavelength dependent form of Δk. This can be achieved by adjusting the non-collinear angle [32]. Fortunately, for the chosen non-collinear angle, OPA adds large positive contributions to the TOD and FOD, which offsets the negative starting values from the prism stretcher (Table 3). Also intense pumping of the nonlinear crystals, with correspondingly smaller crystal lengths, generally reduces the change in phase caused by OPA, compared to moderate pumping and longer crystals (results not shown).

The contribution of PM compared to the other two effects is generally smaller. From Eq. (2), it would be expected that the *B*-integral for the signal after the first stage is approximately 0.77 for both LBO and BBO. This result is dominated by the large intensity of the pump pulse. However, if the signal pulse duration is smaller than the pump pulse duration, the signal experiences a largely "flat" pump pulse. Therefore cross PM from pump to signal only adds a relatively constant phase to the signal. This is complicated because the pump pulse undergoes a large depletion, which adds an inverted phase modulation to the signal. The combined processes are rather complex, depending on intensity of the signal and pump pulses, length of crystals, the degree of pump depletion, and exact details of the relative timing, spatial and spectral parameters of the two input pulses (signal and pump). Therefore, instead of using Eq. (2) to measure the effects of phase modulation on the signal pulse, it is better to examine the change phase modulation adds to each dispersion order. As an example, the changes of spectral phase in LBO for the second, third, and fourth order are given in Table 3 for all three stages. The changes in phase due to phase modulation are much smaller than the contributions due to the dispersion for GDD and TOD, however, for the FOD they are similar. Using the chosen parameters in this design, phase modulation has only minor effects on both the output signal energy and bandwidth.

6. Pulse Energetics and Thermal Effects

Having established pump-to-signal conversion efficiencies of over 20% for LBO and BBO, for a given bandwidth and spatial beam quality at pulse energies near 1 mJ, the complete pulse energetics can now be summarized. If it is assumed that second harmonic generation (SHG) in a LBO crystal has an efficiency near 50% and a OPCPA-pump pulse of 8 mJ at 515 nm is required (Fig. 1), then the starting pulse energy of the fundamental (1030 nm) needs to be $\sim$16 mJ. Therefore, the required OPCPA-pump power at the fundamental of 1030 nm is $0.016 \times f_r$, where f_r is the pulse repetition rate (discussed below).

The maximum average power, or corresponding repetition rate (f_r), is then finally determined by the thermal properties of LBO and BBO. Although the OPCPA process does not involve direct absorption of energy through a change of quantum numbers, there is residual absorption modeled by the Beer-Lambert law with coefficients (α) that are frequency dependent (Table 1). A rough estimate of the amount of power (P) to be dissipated through a crystal is given by the equation $P = f_r \tau I_{max} \alpha L \pi (D/2)^2$, where L is the length of the crystals and the other parameters are defined in Tables 1 and 2. In the simulations, narrow band pump-pulse absorption was calculated within the solution of the nonlinear equations (Eq. (1)). The frequency dependent absorption parameters of the signal and idler pulses were taken from [17] (see Fig. 6), and were calculated in the frequency domain. For both LBO and BBO the full bandwidth of the Ti:sapphire oscillator (i.e. the signal pulse) has almost 100% transmission across its full bandwidth. However, the idler pulse, calculated by $1/\lambda_I = 1/\lambda_P - 1/\lambda_S$, extends well into wavelengths above 2000 nm, if the full bandwidth of the oscillator is used. Therefore, in the simulations, a lower wavelength cut-off was used on the initial signal pulse to restrict large attenuation of the idler pulse. Note: BBO allows a slightly greater bandwidth window, with reduced signal and idler adsorption, compared to LBO (Fig. 6). However, there are less restrictions on the idler attenuation, if the signal pulse from the Ti:sapphire oscillator could be

#198661 - $15.00 USD Received 30 Sep 2013; revised 27 Nov 2013; accepted 27 Nov 2013; published 16 Jan 2014

broadened beyond wavelengths of 1100 nm. This is not considered in this work, but has been experimentally achieved [3].

The second OPCPA stage absorbs the most laser pulse energy, and therefore sets the limits on the maximum average output power. The second stage heat load for LBO/BBO integrated over the whole crystals was calculated to be 88 / 40, 35 / 5, and 1080 / 6390 [nJ / per pulse] for the signal, idler, and pump pulses, respectively. The pump pulse absorption is the major source of crystal heating. Significant heating can be caused by the idler pulses if it is allowed to go beyond 2000 nm, as was recently demonstrated in BBO [14].

In order to estimate the change in temperature across the crystal, a simple model of a crystal holder was used, which has a heat sink around the edge of the crystal and considers only a radial heat flow [33]. At a repetition rate of 100 kHz, the results of this model are shown in Fig. 7 for the second LBO stage, using parameters from the simulation and material parameters from Table 1. Ideally, to prevent a loss of phase matching or to maintain spatial beam quality, a constant temperature profile across the laser beams would be required. In the radial dimension (x-axis), minimizing changes in temperature might be realized by a careful design of the crystal holder. Keeping a near constant temperature along the z-axis can be achieved by balancing heat profiles from the signal, idler and pump. Towards the end of the crystal, the pump pulse becomes depleted, while the energy of the signal and idler pulses increases. In Fig. 7, the maximum temperature increase at the input side of the crystals was 8.9 K, and increases to 11.5 K at the output side for LBO, due to a greater increase of heating from the signal and idler pulses compared to the pump pulse. Applying this temperature profile in the simulation code, only minor changes ($\sim$1%) to the critical parameters, signal energy, bandwidth, and M^2, were observed, compared to a flat temperature profile at the maximum temperature. Thus, we can predict a lower conservative limit where thermal effects start to affect the laser performance. Using the LBO parameters from Table 2, the simulated OPCPA amplifier can achieve 181 W at 100 kHz with 7 fs pulses with minimal temperature effects, requiring an OPCPA-pump of around 1.6 kW at 1030 nm.

Using this thermal model for the crystal holder, the maximum change in temperature is proportional to $f_r \alpha E/\kappa$. Thus for the same pulse energy E and repetition rate f_r, BBO has approximately 26 times greater temperature increase as LBO at 515 nm (Table 1). Repeating the thermal simulation for BBO, the maximum change in temperature for BBO was 205 K, at 100 kHz. In compensation to this large change of temperature, the phase matching temperature tolerance $\delta T \cdot l$ is 8.7 times better than LBO (Table 1). However, what is not considered

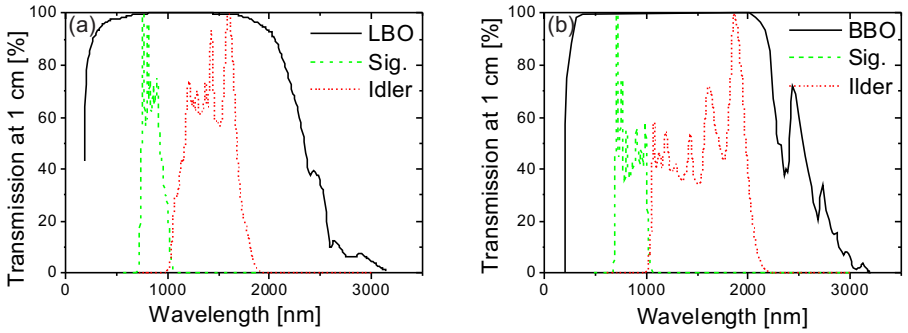

Fig. 6. Optical transmission in dependence on wavelength [17], and spectra of signal and idler pulses at the end of the second stage for both LBO (a) and BBO (b).

#198661 - $15.00 USD Received 30 Sep 2013; revised 27 Nov 2013; accepted 27 Nov 2013; published 16 Jan 2014

with this simple model is the effect of a large temperature gradient within the crystal, which will cause large differential expansion resulting in large strains. These considerations, including a more detailed thermal model of the crystal holder, are beyond the scope of this paper. We therefore suggest that BBO would be ideal for burst-mode operation. In addition, BBO has a larger gain bandwidth compared to LBO. For example, at the new FEL, FLASH 2 at Hamburg, a three-stage BBO OPCPA system is planned for burst-mode operation (up to 1 MHz for 800 µs at 10 Hz). The average power of this system effectively corresponds to a repetition rate of 8 kHz, where thermal effects can be neglected.

7. Discussion and Conclusion

A design study was carried out for a high power, ultrabroadband, three-stage OPCPA with sub-7.0 fs pulses with energies above 1mJ, comparing the nonlinear crystals LBO and BBO. The design parameters discussed in this work require OPCPA-pump amplifiers above one kilowatt delivering sub-1 ps pulse durations at 1030 nm in continuous mode operation. Currently, there are no commercially available OPCPA-pump amplifiers with these parameters. However, realization of the next generation of high repetition rate, ultrabroadband OPCPAs depends on this development. Because the OPCPA-pump is often the most costly part of the complete OPCPA amplifier, this paper has explored the most effective use of the pump pulse energy and signal beam characteristics in a three-stage OPCPA.

The main results without thermal effects can be summarized. Both crystals, LBO and BBO, can amplify signal pulses to energies more than 1 mJ, with bandwidths that support signal pulses of sub-7 fs, and with signal-to-pump conversion efficiencies above 20% in a three-stage OPCPA system. Additionally, given the choice of input signal spectrum (Figs. 3 and 6), the bandwidth of the OPCPA, especially of LBO, could be improved by using either (i) larger pump intensities at each of the three stages, and (ii) reducing ratio of signal pulse duration compared to pump pulse duration, with a slight reduction in pump-to-signal conversion efficiency. The beam

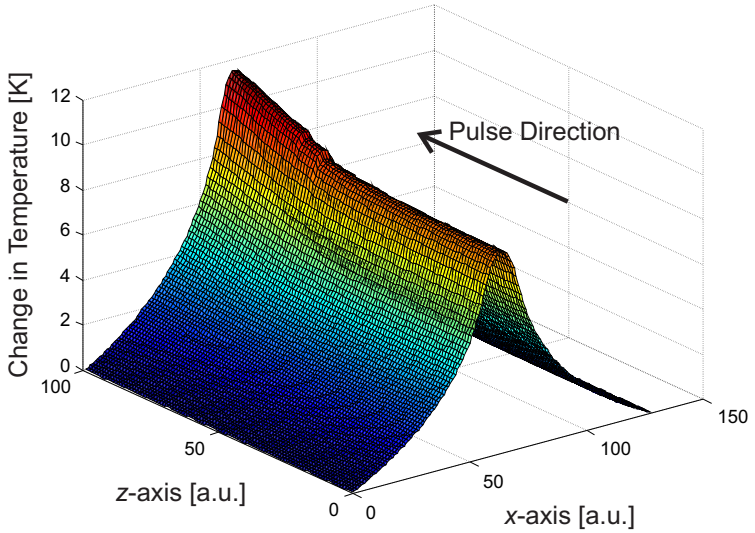

Fig. 7. A 2 dimension (x,z) simulation of the change of temperature profile across the crystal of the second stage of the OPCPA for LBO. The laser passes along the z-axis (arbitrary units), with one transverse direction x (arbitrary units). At the edge of the crystal along the x-axis is assumed to have an idealized heat sink.

#198661 - $15.00 USD Received 30 Sep 2013; revised 27 Nov 2013; accepted 27 Nov 2013; published 16 Jan 2014

profiles were analyzed throughout the three-stage amplifier and M^2-values were calculated at the end of each stage. Final M^2-values of 1.2 can be achieved, assuming Gaussian pump beams. The relationship between the signal and pump beam profiles has been explored at each of the three stages. It is expected that the final beam quality is largely determined by the intensity of the pump beam through the nonlinear crystal and not its spatial phase. Thus, with careful adjustment of the OPCPA system and good near-field pump beam quality, a three-stage OPCPA can provide good spatial beam quality of the signal. The spectral phase of the signal does not appear to be adversely affected by either the OPCPA process or by self- and cross-phase modulation, provided that each stage is correctly adjusted (Section 5) and is not driven too hard causing back conversion. Note: This is a highly complex system to optimize and no attempt was made to find the maximal optimum efficiency within the given goals and restrictions.

The ultimate limits on the output from a single OPCPA stage are given by the thermal effects. For both crystals, greater signal bandwidth can be provided by extending the signal spectrum into the near infrared, without causing any detrimental heating effects (Fig. 6). In this case, the idler spectrum would be extended to lower wavelengths where there is less absorption. For continuous mode operation, LBO would be the crystal of choice, largely because it has a smaller α/κ ratio compared to BBO. BBO is a good choice for burst-mode operation, because it has a broader gain-bandwidth and a broader transmission window (Fig. 6). Additionally, in this three-stage OPCPA, the second stage suffers the highest heat load, and therefore this stage was analyzed in more detail (Fig. 7). In continuous mode operation, no attempt was made to find a maximum final output power, because this would require a detailed model of the crystal holder and knowledge of the behavior of the nonlinear crystal with large temperature variation across the crystal. This latter effect will lead to differential expansion and large strains within the crystal, which are difficult to predict: most parameters are measured at constant temperature. We have therefore decided to restrict the maximum change in temperature for LBO to ~ 10 K, where only minor changes were observed in the critical laser parameters. We also provide strategies for minimizing heat absorption, demonstrating an almost constant temperature through the length of the crystal along the z-axis, which is achieved by a careful balance of the signal and corresponding idler spectrum (Figs. 6 and 7). Using these assumptions and a conservative estimate of the material parameters (Table 2), an estimate of the final signal output power of 181 W with sub-7 fs pulses can be achieved using LBO at 100 kHz repetition rate. At these powers, we expect thermal effects to have negligible affects on the critical laser parameters.

Acknowledgment

The authors would like to thank the financial support of the Helmholtz-Institut Jena and the Photon Science department of Deutsches Elektronensynchrotron DESY in Hamburg.

#198661 - $15.00 USD Received 30 Sep 2013; revised 27 Nov 2013; accepted 27 Nov 2013; published 16 Jan 2014